

Study of Slip Flow in Unconventional Shale Rocks using Lattice Boltzmann Method: Effects of Boundary Conditions and TMAC

Rasoul Nazari Moghaddam, Mahmoud Jamiolahmady
Institute of Petroleum Engineering, Heriot-Watt University, UK

Abstract

Development and production from unconventional resources require understanding of flow mechanisms and rock/fluid interactions, which are different from those in conventional reservoirs. Several flow regimes including slip and transition can be dominated in these reservoirs due to the presence of micro and nano-pores. Recently the lattice Boltzmann method (LBM) has been considered as a well-accepted method for simulation of slip flow in shale rocks. In this paper, the two-relaxation-time (TRT) based Lattice Boltzmann approach was adopted to simulate the slip flow in a single channel and a simplified 2D and 3D porous media. Different boundary conditions including diffusive reflective (DR) and bounce back-specular reflection (BSR) were used to capture the gas slippage at the wall surface. The simulation results were compared with the experimental data measured on three shale rock samples. The results showed that the gas slippage in the shale samples under study cannot be modelled using the literature tangential momentum accommodation coefficient (TMAC) values. It was also shown that the permeability enhancement was overestimated for $Kn > 0.1$ when the gas flow was simulated in a single channel. Furthermore, from the fitted line to the simulation results (up to $Kn = 0.3$), the first and second order slip coefficients of the N-S boundary conditions were found as 2 and 1.54, respectively.

Keywords

Unconventional reservoirs, Shale rock, 3D Lattice Boltzmann, Slip flow, Klinkenberg, Knudsen number

Introduction

The growing energy demand on one side and the continuance of fossil fuels as the main source of energy on the other side highlight the important role of the unconventional reservoirs in global energy markets in future. The main characteristic of the unconventional reservoirs is their low matrix permeability. Fluid flow in low-permeability unconventional reservoirs is a more complex process and subject to more nonlinear physical processes compared to flow in conventional reservoirs. The presence

of micro- and nano-pores in such matrices makes the dynamics of fluids flow and their interaction with surfaces to be very different from those in conventional systems.

In micro- and nano-pore systems, the mean free path (MFP) of the flowing gas molecules are significant relative to the dimensions of the flow conduit. As a result, the impact of the Knudsen layer, which is a local non-equilibrium area near the wall surface, on the overall flow performance increases. A widely recognized dimensionless parameter that characterises the resultant different flow regime is Knudsen number (Kn). It is defined as the ratio of the molecular mean free path (λ) to a representative characteristic length (L). Based on the Knudsen number of the system, the gas flow regime can be continuum flow ($Kn < 0.01$), slip flow ($0.01 < Kn < 0.1$), transition flow ($0.1 < Kn < 10$), and free molecular flow ($Kn > 10$). As the Knudsen number increases, the validity of the standard continuum approach for the Navier-Stokes (N-S) equations diminishes. At such conditions, the Darcy's law cannot be used to characterize the permeability as it has been derived from N-S equations. Hence accurate permeability estimation is required (by considering the flow regimes) to improve the gas flow prediction. It should be noted that gas flow in Unconventional Gas Reservoirs (UGRs) is mainly considered to be either under slip flow or transitional flow regimes, depending on the size of pores, pressure, type of gas molecules and etc (Freeman et al. 2011; Kang et al. 2011; Sinha et al. 2013; Heller et al. 2014; Yves et al. 2015; Ghanizadeh et al. 2014).

To model slip flow in shale gas reservoirs, researchers have used two mathematical approaches to describe the gas transport and calculate gas apparent permeability. The first approach is to solve the N-S equation with the non-slip boundary conditions (Florence et al. 2007; Sakhaee-Pour, Bryant 2012; Civan 2010; Ziarani, Aguilera 2012). Their works are mainly based on the Beskok-Karniadakis unified model (Beskok, Karniadakis 1999). In almost all models in this category, the proposed Beskok-Karniadakis unified model with the same slip and tangential momentum accommodation coefficient (TMAC), which has been proposed for low pressure gas flow in a single straight pipe, have been used. The second approach is the Dusty Gas Model (DGM) model, which assumes a linear combination of the viscous flow and the gas diffusion to predict the overall flow rate in micro and nano-pores (Javadpour 2009; Darabi et al. 2012; Deng et al. 2014; Guo et al. 2015). However there are reported documents that shows the DGM model is not accurate enough, when strong potential energy gradients exist, which is mainly because the Knudsen diffusivity is based on the simple kinetic theory (Niu et al. 2014; Bhatia, Nicholson 2003; Bhatia et al. 2011).

The mentioned studies have received some attentions and resulted in better prediction of the UGRs matrix permeability, but almost all these analytical and semi-analytical solutions were originally developed based on simple geometries such as channels or tubes. Hence for more complex flow path systems (e.g. porous media), they can only provide an approximate solution. Recently, the Lattice Boltzmann Method (LBM) has received attentions for such applications. It solves a discretized form of the continuous Boltzmann equation, which is an accepted relationship for modelling the evolution of gas flow based on the kinetic theory of gas particles, for a regular lattice. This technique is computationally efficient as it deals with particle distribution functions. In fact, the intrinsic kinetic nature of the LBM makes it an attractive method for microfluidic flows with high Knudsen numbers similar to the gas flow in shale and tight matrices. In the LBM, to account the slippage at the wall surface, the interaction of gas particles with solid surface should be defined properly through the solid boundary conditions.

To date, different boundary conditions have been proposed for this purpose such as bounce back (Nie et al. 2002), specular reflection (Lim et al. 2002; Succi 2002), diffusive reflection and combinations of them (Sofonea, Sekerka 2005). Sbragaglia and Succi (2005) derived analytical expressions for a broad class of boundary conditions for the slip flow and compared the corresponding results with numerical simulations (Sbragaglia, Succi 2005). Sofonea and Sekerka (2005) also studied the effect of various boundary conditions including bounce back, specular reflective and diffusive reflective (Sofonea, Sekerka 2005). In addition to different boundary conditions, different relaxation time models have been also used in the literature. The relaxation time is a constant which determines the microscopic dynamics towards the local equilibrium and the macroscopic transport coefficients at the same time. In the LBM (a mesoscopic model) the relaxation time is the practical tuneable parameter which can be set in order to recover the desired dynamics, both microscopic and macroscopic (Asinari 2005). Although most of these studies were based on single relaxation time (SRT) model (Niu et al. 2004; Zhang et al. 2005; Guo et al. 2006; Homayoon et al. 2011; Shokouhmand, Isfahani 2011; Tang et al. 2005), multi relaxation time (MRT) and two relaxation time (TRT) (Guo et al. 2008; Li et al. 2011; Verhaeghe et al. 2009; Ginzburg et al. 2008) have been also used for slip flow studies. The main reason of using TRT and MRT is the deficiency of the SRT model for slip flow simulations as mentioned by Luo (Luo 2004, 2011). He argued that slip velocity predicted by SRT with bounce-back boundary condition is merely numerical artefact. Verhaeghe et al. (2009) have also

shown that two relaxation times (TRT) is as efficient as the corresponding STR-LB models. In other words, TRT model is similar to SRT model in simplicity and efficiency, but still retains the advantages of MRT model in terms of accuracy and stability (Verhaeghe et al. 2009).

Some LBM simulations have been published recently regarding gas flow in tight and shale formations. Using LBM, Fathi et al. (2012) showed that inelastic collisions of gas molecules with the nano-capillary walls create a high kinetic energy molecular streaming effect on the fluid flow. This leads to dramatic changes in the fluid flow velocity profile (Fathi et al. 2012). Fathi and Akkutlu (2013) performed LBM simulations with a Langmuir slip boundary condition to incorporate the slippage and the surface-transport mechanisms. They introduced the surface transport of the adsorbed phase as a moving wall in the model (Fathi, Akkutlu 2013). Zhang et al. (2015) performed Lattice Boltzmann simulations and proposed a method to estimate the matrix permeability of complex pore structures. They investigated various possible factors that affect shale gas flow characteristics and analysed the influence of each factor (Zhang et al. 2015). Ren et al. (2015) applied the Langmuir isothermal adsorption equation with bounce-back/specular-reflection boundary conditions, to take into account the effects of surface diffusion, gas slippage and adsorbed layer (Ren et al. 2015). Ning et al. (2015) propose a method to incorporate inter-molecular and adsorptive forces into the generalised LBM algorithm to capture gas adsorptions in organic nano-pores (Ning et al. 2015).

In all studies mentioned above, the strengths and deficiencies of the LBM for simulation of gas flow in shale gas reservoirs have not been well addressed. In addition, the simulation results of LBM have never been scaled and compared with actual shale rock experimental data measured at high pressure.

In this research, for the first time, various slip boundary conditions were employed in the LBM to consider the gas slippage in porous media. The two-relaxation-time (TRT) lattice Boltzmann method has been used in this study to simulate the gas flow in a single channel, a pore body / pore throat system and a simplified 3D porous medium. The results of LBM were verified for slip flow, based on the solution of other methods (IP and DSMC). After this validation step, the slip boundary conditions were applied and the simulation results of slip flow were compared by the scaled experimental data. As the simulation results were compared with the scaled experimental data, the suitability of different boundary conditions for simulation of gas flow in shale rock was investigated. Furthermore comparison of the experimental data and simulation results

were used to obtain appropriate TMAC value for LBM simulation of gas flow in shale rocks. The TMAC value is an important factor as the slippage intensity can be determined by this coefficient in shale matrices.

Methodology

Lattice Boltzmann Method (LBM)

The Lattice Boltzmann method (LBM) simplifies the Boltzmann's original idea of gas dynamics by considering a reduced number of particles confined in the nodes of a lattice. For example, in a two-dimensional model, a particle is restricted to stream in nine possible directions. These velocities are referred to as the microscopic velocities and denoted by \vec{c}_α , where $\alpha = 1, \dots, 8, 9$. Figure 1 shows this model referred to as D2Q9 for this two dimensional geometry with nine possible paths. As shown, lattice nodes are assumed and the fluid particles can move to the neighbour nodes. For each particle on the lattice, nine discrete distribution functions $f_\alpha(x, t)$ is considered, which describe the probability of streaming in different directions. As shown in this figure, the particle can move to the neighbour nodes (eight nodes and itself) in each streaming step. In the case of D3Q19 lattice model, a particle is restricted to stream in 18 possible directions. For each particle in D3Q19 lattice, 18 discrete distribution functions $f_\alpha(x, t)$ is considered, which describe the probability of streaming in different directions. Figure 2 shows the schematic of D3Q19 lattice and the 18 possible streaming directions.

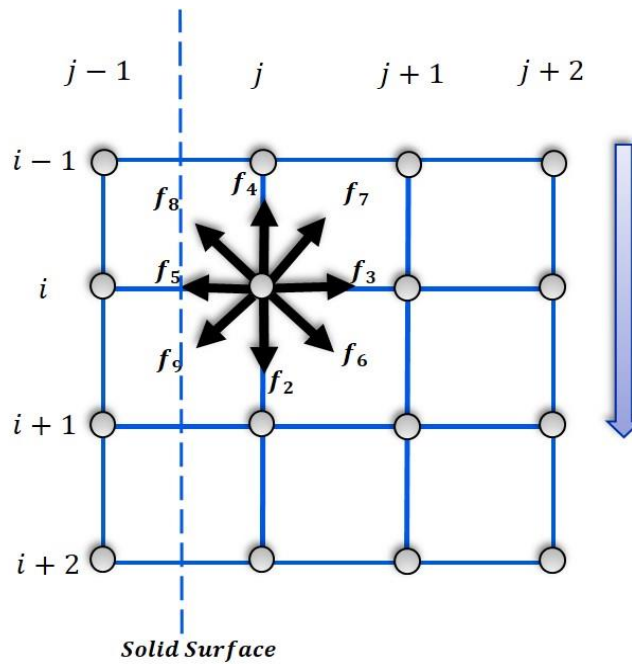


Figure 1: The Schematic of the boundary nodes near the wall and the corresponding distributions used for different boundary conditions implemented for gas flow simulations.

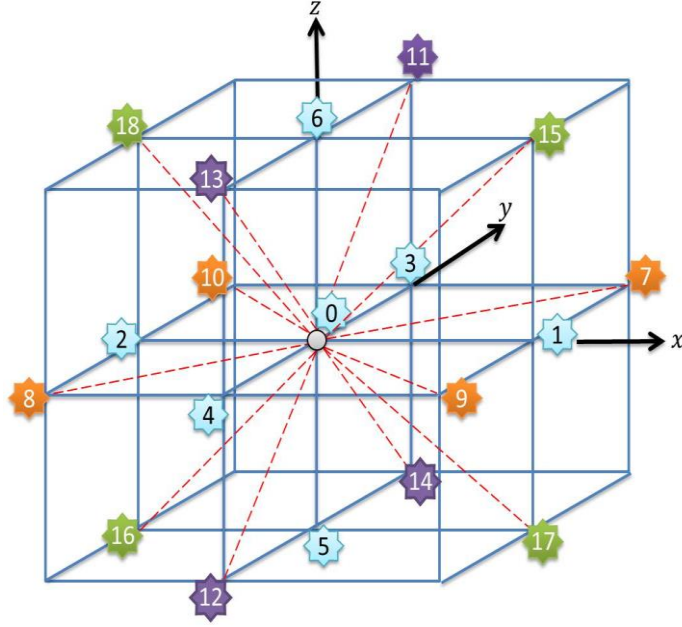


Figure 2: The schematic of D3Q19 lattice and the corresponding streaming directions.

The macroscopic fluid density of each particle is defined as a summation of microscopic particle distribution function:

$$\rho(x, t) = \sum_{\alpha=0}^{\alpha=N} f_{\alpha}(x, t) \quad (1)$$

where N is the maximum number of possible streaming directions. Accordingly, the macroscopic velocity $\vec{u}(x, t)$ is an average of microscopic velocities \vec{c}_i weighted by the distribution functions (f_{α}):

$$u(x, t) = \frac{1}{\rho} \sum_{\alpha=0}^{\alpha=N} \mathbf{c} f_{\alpha} \vec{c}_i \quad (2)$$

where \mathbf{c} is the lattice speed for fluid particles moving from site to site, expressed as $c = \Delta x / \Delta t$. The equilibrium distribution (f_{α}^{eq}) in the LBM can be expressed by expanding the exponential function in Boltzmann-Maxwell distribution function into a Taylor series expansion as (Satoh 2010):

$$f_{\alpha}^{eq} = \rho w_{\alpha} \left[1 + b \frac{c_{\alpha} \cdot u}{c^2} + e \frac{u^2}{c^2} + h \frac{(c_{\alpha} \cdot u)^2}{c^4} \right] \quad (3)$$

where w_{α} , b , e and h are the constants, which should be determined based on the model dimensions (e.g. D2Q9, D3Q19, etc). It is noted that these parameters should be determined such that the terms on the right hand sides of Equations 1 and 2 remain

unchanged by a rotation of the whole lattice system by an angle of ϕ (Satoh 2010). For D2Q9 model, these parameters are obtained as:

$$w_\alpha = \begin{cases} \frac{4}{9} & \text{for } \alpha = 0 \\ \frac{1}{9} & \text{for } \alpha = 1, 2, 3, 4 \\ \frac{1}{36} & \text{for } \alpha = 5, 6, 7, 8 \end{cases}, \quad (4)$$

and $b = 3$, $e = -3/2$, $h = 9/2$. For D3Q19 model, these parameters are:

$$w_\alpha = \begin{cases} \frac{1}{3} & \text{for } \alpha = 0 \\ \frac{1}{18} & \text{for } \alpha = 1, \dots, 6 \\ \frac{1}{36} & \text{for } \alpha = 7, \dots, 18 \end{cases}, \quad (5)$$

and $b = 3$, $e = -3/2$, $h = 9/2$. The key steps in standard LBM are the streaming and collision processes as given by:

$$f_\alpha(x + \Delta x, t + \Delta t) - f_\alpha(x, t) = -\frac{1}{\tau} [f_\alpha(x, t) - f_\alpha^{eq}(x, t)] \quad (6)$$

or

$$f_\alpha(x + \Delta x, t + \Delta t) = \frac{1}{\tau} [f_\alpha^{eq}(x, t)] + (1 - \frac{1}{\tau}) f_\alpha(x, t) \quad (7)$$

where τ is the relaxation time and it is related to the fluid kinematic viscosity (ν), which is expressed by:

$$\nu = \frac{2\tau - 1}{6} \frac{(\Delta x)^2}{\Delta t} \quad (8)$$

As mentioned, TRT lattice Boltzmann method was used in this study. In two-relaxation-time (TRT-LBM) scheme, the distribution function is divided into two parts of symmetric and antisymmetric as follow (Ginzburg 2005; Mohamad 2011):

$$f_\alpha^S = \frac{1}{2} (f_\alpha + f_{-\alpha}) \quad (9)$$

and

$$f_{\alpha}^{AS} = \frac{1}{2} (f_{\alpha} - f_{-\alpha}) \quad (10)$$

where f_{α} is the distribution function moving opposite to the $f_{-\alpha}$. Therefore the collision equation can be expressed by:

$$\begin{aligned} & f_{\alpha}(x + \Delta x, t + \Delta t) - f_{\alpha}(x, t) \\ &= -\frac{1}{\tau_S} (f_{\alpha}^S(x, t) - f_{\alpha}^{Seq}(x, t)) - \frac{1}{\tau_{AS}} (f_{\alpha}^{AS}(x, t) \\ & - f_{\alpha}^{ASeq}(x, t)) \end{aligned} \quad (11)$$

where

$$\frac{1}{\tau_S} = \omega_S = \frac{1}{3v + 0.5} \quad (12)$$

where ω_S and ω_{AS} are the symmetric and asymmetric collision frequencies, respectively. The asymmetric collision frequency is related to symmetric collision frequency as follows:

$$\omega_S = \frac{8(2 - \omega_{AS})}{8 - \omega_{AS}} \quad (13)$$

In this study, the Knudsen number of the system is also calculated based on the definition of Zhang et al. (2005). As the mean free path can be reduced in confined system, effective mean free path should be used in association with relaxation time calculation. As shown by Tang et al. (2008), the relaxation time is related to bulk Knudsen number (Kn_0) and effective mean free path as follow(Tang et al. 2008):

$$\tau = \left(\frac{\lambda}{\lambda_0}\right) \sqrt{\frac{\pi}{8}} \left(\frac{c}{c_s}\right) Kn_0 N_L + 0.5 \quad (14)$$

where λ and λ_0 are effective and bulk mean free paths. c and c_s are lattice velocity and speed of sound in the lattice. N_L is equal to H/lu where lu is lattice length or lattice unit. Therefore, the Knudsen number is related to relaxation time as follows (Zhang et al. 2005):

$$Kn = \sqrt{\frac{8}{3\pi}} \frac{\tau - 0.5}{H} \quad (15)$$

where H is the characteristic length of the system which is node number here. It has to be added that for all simulations in this study, the constant pressure (density) boundary conditions (Zou,He 1997) were used to be in line with the performed experiments.

Solid-gas Slip Boundary Conditions

As indicated before, to account the molecular slippage on the wall surface, appropriate boundary conditions (BCs) are required to be defined in the lattice Boltzmann simulation of slip flow. It is very important to address how the gas molecule should be reflected after collision with wall surface. For this purpose, after each streaming step, the distribution functions of boundary nodes (i.e. nearest nodes to the wall surface) should be updated to address the appropriate molecular reflection with slippage. In other words, the discrete distribution functions on the wall boundaries have to be determined in such a way to reflect the macroscopic BCs. In this study, four different types of boundary conditions, proposed for the solid-gas interaction, were used in the simulations. It is aimed to evaluate the pertinence of the existing boundary conditions for the gas slippage modelling in shale rocks. It is noted that for all simulations in this study, half-way boundary conditions were used. In other words, it is assumed that the distance between solid surface and the boundary nodes is equal to a half lattice unit as shown in Figure 1.

1. Bounce-Back boundary condition (BB)

If a fluid particle (discrete distribution function) reaches a boundary node and scatters back along its incoming direction, the reflection is a bounce-back. In other words, incident particles are reflected in the opposite direction. Accordingly, for the node (i,j) in Figure 1 the following collision process are considered at post stream step :

$$\begin{aligned}
 f_{3, AC}^{i,j} &= f_{5, BC}^{i,j} \\
 f_{6, AC}^{i,j} &= f_{8, BC}^{i,j} \\
 f_{7, AC}^{i,j} &= f_{9, BC}^{i,j}
 \end{aligned}
 \tag{16}$$

where AC and BC refer to “after collision” and “before collision”. It should be noted that f_2 and f_4 are not involved in the boundary condition calculations.

2. Specular Reflection boundary condition (SR)

In this case, the gas particle collides with the wall and specularly reflected such that the angle of incident is equal to the angle of reflection. No shear forces are transmitted and the tangential momentums are conserved. Hence, for the node (i,j) in Figure 1 the following distribution function should be considered for collision process to capture the specular reflection boundary condition.

$$\begin{aligned}
 f_{3, AC}^{i,j} &= f_{5, BC}^{i,j} \\
 f_{6, AC}^{i,j} &= f_{9, BC}^{i-1,j} \\
 f_{7, AC}^{i,j} &= f_{8, BC}^{i+1,j}
 \end{aligned} \tag{17}$$

3. Diffusive Reflection boundary condition (DR)

In this boundary condition, it is assumed that the gas particles are reflected at random angles unrelated to the angle of incident. In this case, the particle velocities reflected from the wall are assumed to follow the Maxwellian distribution law (Cercignani 2000). For this boundary condition, the distribution functions of the three directions, which need to be updated, can be summarised as follows (Sofonea, Sekerka 2005):

$$\begin{aligned}
 f_{3, AC}^{i,j} &= f_{5, BC}^{i,j} \\
 f_{6, AC}^{i,j} &= \frac{f_{7, BC}^{i-1,j} + f_{8, BC}^{i,j} + f_{9, BC}^{i-1,j} - f_{6, BC}^{i,j}}{2} \\
 f_{7, AC}^{i,j} &= \frac{f_{6, BC}^{i+1,j} + f_{9, BC}^{i,j} + f_{8, BC}^{i+1,j} - f_{7, BC}^{i,j}}{2}
 \end{aligned} \tag{18}$$

4. Bounce-back Specular Reflection boundary condition (BSR)

This boundary condition, which was proposed by Succi, allows the gas particle to bounce back and to be specularly reflected with probabilities equal to (r) and ($1 - r$), respectively (Succi 2002). The case $r = 1$ corresponds to the fully bounce-back rule while $r = 0$ captures the fully specular boundary condition. This boundary condition provides a free adjustable parameter to model slip flow phenomena (Zhu et al. 2005; Zhang et al. 2005). Sbragaglia and Succi have shown the relationship between this parameter (r) and the tangential momentum accommodation coefficient (Sbragaglia, Succi 2005). As shown, the slip coefficient in Maxwellian type slip models can be obtained as follows:

$$A = \frac{c}{c_s} \frac{1 - r}{r} \tag{19}$$

where c and c_s are the lattice speed and speed of sound, respectively, and A is related to the tangential momentum accommodation coefficient, TMAC, (σ) as, $A = \frac{2-\sigma}{\sigma}$.

It is noted that, for all simulations, mid grid configuration was used for modelling the solid boundary conditions. In this configuration, as can be seen in Figure 1, imaginary nodes are assumed (column $j - 1$) such that the wall surface is at the centre of these imaginary and boundary nodes. Therefore, the boundary nodes (column j) are the nearest nodes to the wall surface.

Experiments

In this paper, the simulation results were compared with our experimental data published recently. In these experiments, several coreflooding experiments were performed to study the gas flow in the unconventional shale reservoir rocks. These experiments include several steady state and unsteady state gas permeability measurements performed on three different shale rock types at different pore pressures. The experiments were designed such that the gas flow regimes were in the slip and a small part of the transition region ($0.01 < Kn < 0.3$). The measured apparent permeabilities were then scaled using the calculated non-slip permeability through the Klinkenberg correction. A so-called “general slip plot” was then generated representing the dimensionless permeability (K_D) values versus the Knudsen number of the experiments. To calculate the Knudsen number, the average of pore sizes obtained from the MICP experiments were used. The obtained dimensionless slip plot is shown in Figure 3. This dimensionless plot shows the effects of gas slippage on the enhanced permeability of shale samples irrespective of the rock type. It is noted that this permeability enhancement factor (dimensionless) is the ratio of the absolute permeability with and without gas slippage. As the other rock properties such as tortuosity, pore size distribution, porosity and etc were the same for both measurements, the permeability enhancement factor (K_D) is not a function of these properties. In other words, this factor indicates the improvement of the permeability due to gas slippage only.

In this study, the LBM simulation results were compared with the data shown in this figure which obtained through the experimental measurements. More details about the experimental conditions, procedures and the results can be found elsewhere (Nazari Moghaddam, Jamiolahmady 2016b, a).

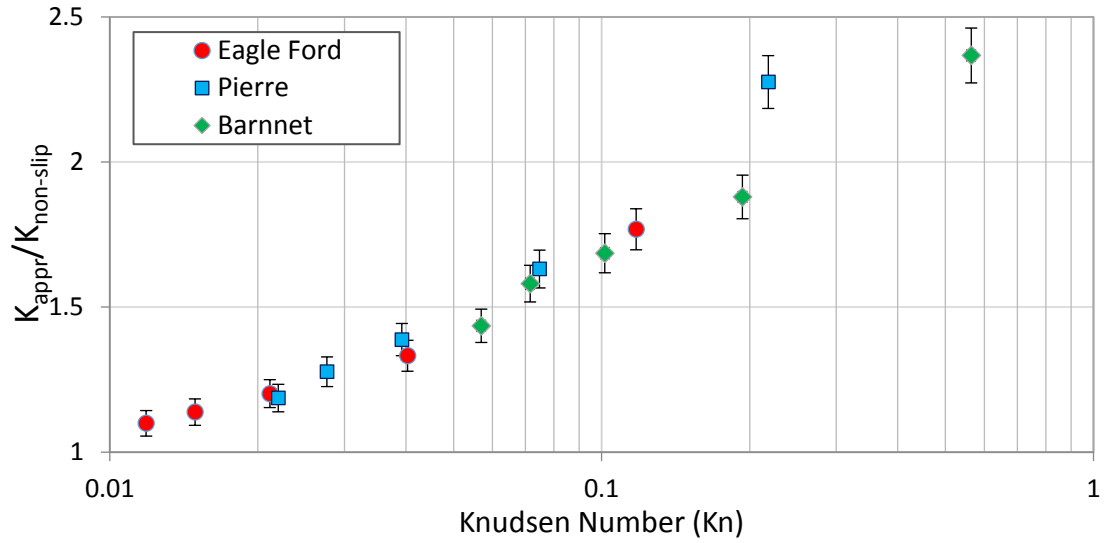


Figure 3: Dimensionless permeability versus Knudsen number for three shale plugs.

Results and Discussion

Validation of the LBM simulation results

The simulation results of the LBM were initially validated for non-slip gas flow in a channel. To this aim, the obtained velocity profile were compared with the analytical solution of the Navier-Stocks equation for non-slip gas flow. In these simulations, as the flow is in the continuum regime (non-slip), the molecular collisions at the wall boundaries should follow bounce back reflection (BB) which is equivalent to zero slip velocity at the wall surface. Figure 4 shows the simulation results of velocity profile in a channel (wall to wall) and the obtained values from the analytical solution of N-S equation (Bao,Meskas 2011). As can be seen, the velocity profile predicted by LBM simulation is in good agreement with the exact solution of N-S equation. It is noted that the gas velocity at wall surface is zero for both cases. In addition, grid sensitivity was performed to investigate the effects of grid number on simulation results. As shown in Figure 5, the obtained dimensionless velocity profiles are the same for all cases with different grid numbers for channel width.

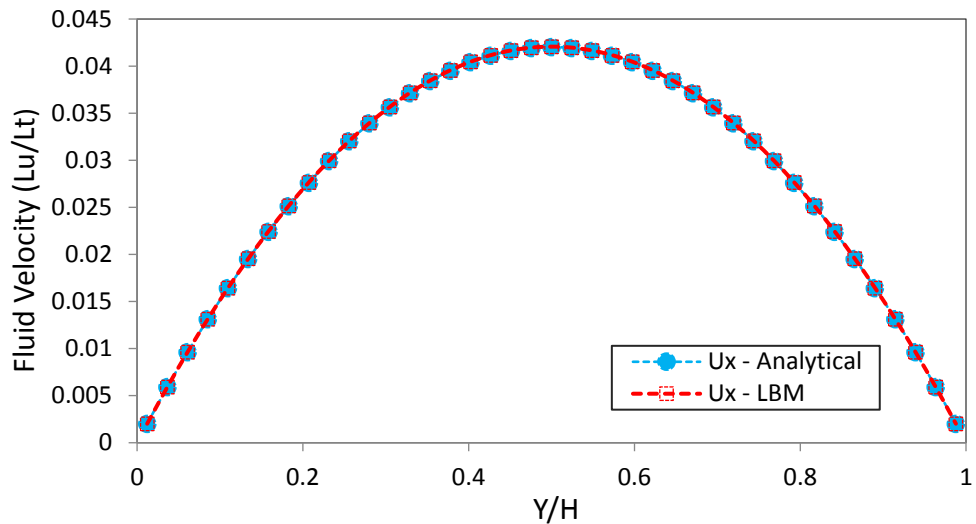


Figure 4: The LBM simulation results of the streamwise velocity profile and the obtained profile from the analytical solution of Navier-Stocks equation for incompressible flow in a channel.

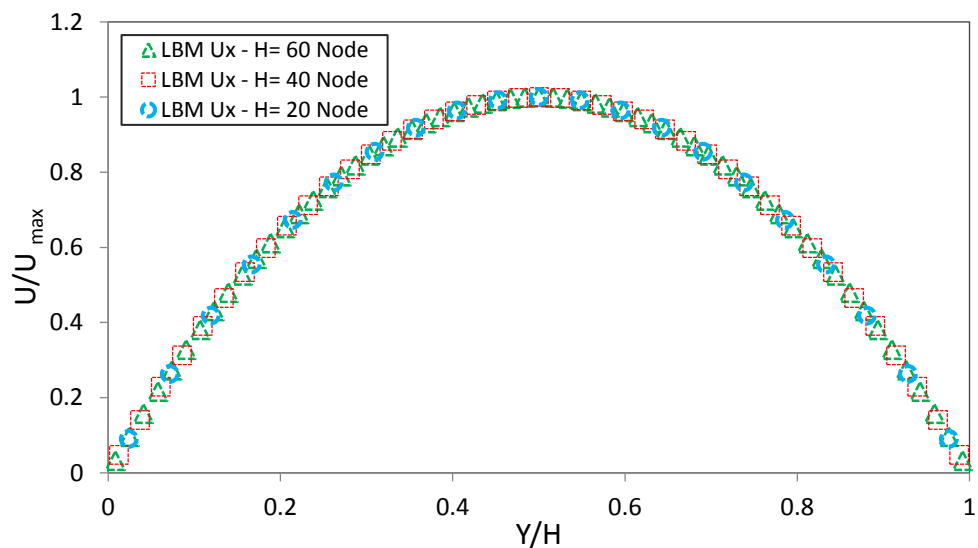


Figure 5: The LBM simulation results of the velocity profile for flow in a single channel using different grid numbers for channel width.

The integrity of simulation results were further confirmed when simulating slip gas flow ($Kn > 0.01$) in a long microchannel. As the main purpose of these simulations was the gas slippage study, the simulation results of gas flow in a long microchannel with slip boundary condition should be validated before any other simulation.

To achieve this aim, slip boundary conditions (as described before) should be activated for simulation of gas flow in a microchannel. In these simulations, two different boundary conditions of diffusive reflection (DR) and Bounce back-Specular reflection (BSR) were used. Then the simulation results were compared with the results

of other simulation techniques such as Direct Simulation Monte Carlo (DSMC) and Information Preservation (IP) methods reported in the literature (Shen et al. 2004). These methods are suitable for modelling slip flow and have been extensively used for such validation purposes (Verhaeghe et al. 2009; Guo et al. 2006). As mentioned before, the two relaxation time (TRT) scheme has been adapted in these simulations. For these validations, the length to height ratio (l/h) was taken to be 100 and the density ratio was $\frac{\rho_{in}}{\rho_{out}} = 1.4$ for $Kn=0.0194$ and $\frac{\rho_{in}}{\rho_{out}} = 2$ for $Kn=0.194$. These particular values of density ratio and Knudsen number were intentionally selected so that the results could be compared by the other methods (Shen et al. 2004). A schematic of the microchannel and the required input data are shown in Figure 6. It is noted that the Knudsen number is calculated using Equation 15. As shown on this figure, the characteristic length was 11 lattice unit (lu) and constant density (constant pressure) was used as boundary conditions (Zou,He 1997).

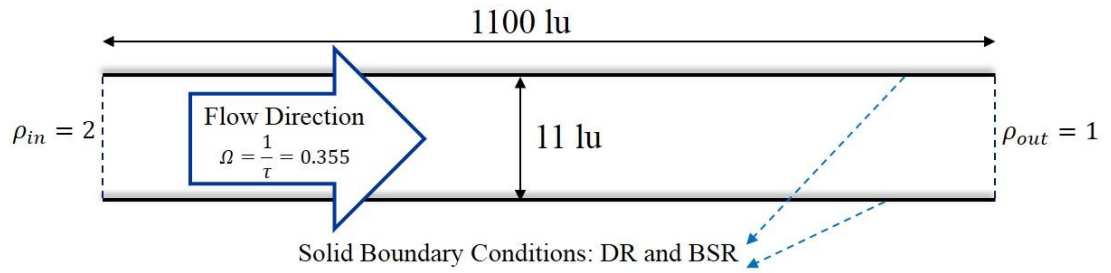
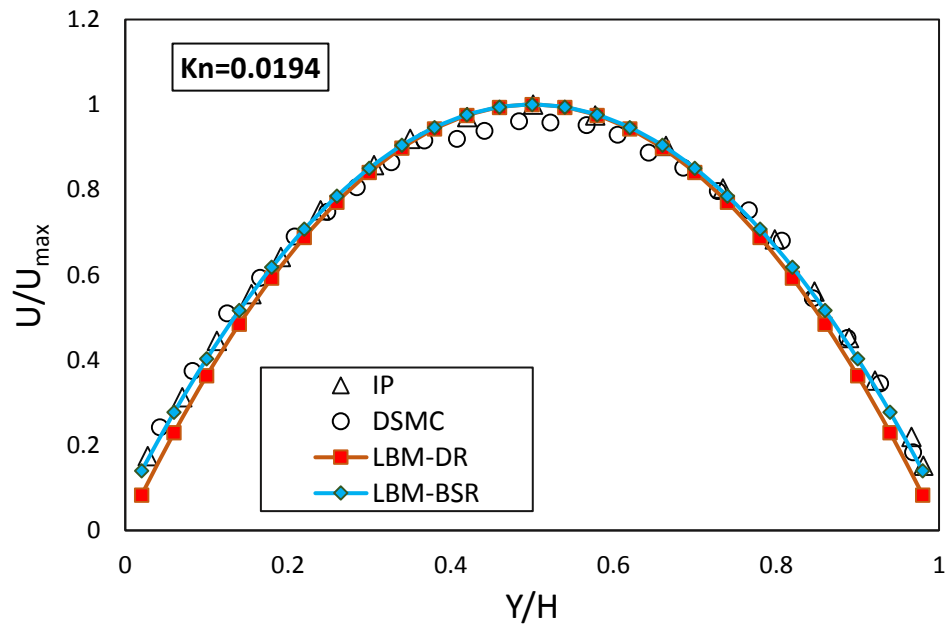


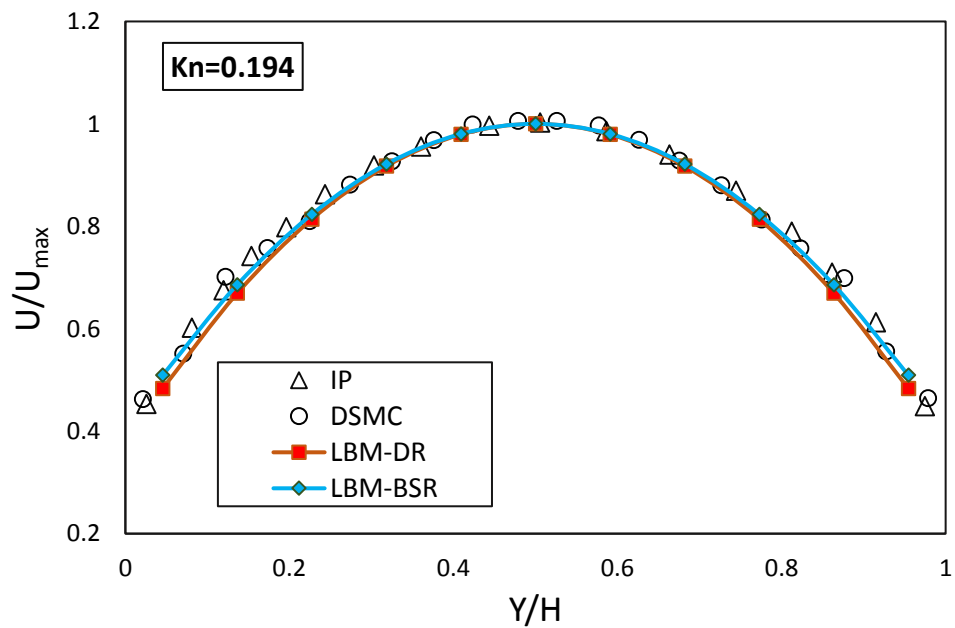
Figure 6: Schematic of the microchannel and the required input parameters.

Figure 7 presents the results of velocity profile across the channel simulated by DSMC, IP (from the literature) and the LBM-DR and LBM-BSR (in this study). The fluid velocities have been normalised by the maximum streamwise velocity at the centre. As shown in this Figure, the LBM results using both DR and BDR boundary conditions agree well with the results of the other two methods available in the literature, i.e. DSMC and IP, at both Knudsen numbers of 0.0194 and 0.194. It should be noted that the r-factor for the BSR boundary condition, which controls the rate of bounce back and specular reflection, should be given to the simulator as an input. In these simulations, an r-factor of 0.54 was given, which is equivalent to the TMAC of 0.8. This value for TMAC is in the range of measured TMAC values for gas flow in microtubes (Maurer et al. 2003; Ewart et al. 2007; Graur et al. 2009). In Figure 7, it is also shown that in addition to LBM-BSR, the DR boundary condition can also properly capture the slippage in a single microtube for these range of Knudsen numbers.

However, it has to be added that the LBM-DR results deviate very slightly from the IP and DSMC results at $Kn=0.0194$.



(a)



(b)

Figure 7: Results of streamwise velocity profile based on Information Preservation (IP), Direct Simulation Monte Carlo (DSMC), LBM-DR and LBM-BSR at a) $Kn=0.0194$ and b) $Kn=0.194$.

Slip Flow in a Single Channel

After validation of slip flow simulations in a microchannel, the developed program was used to generate the general slip plot (similar to Figure 3). As mentioned before, the

general slip plot is a dimensionless graph which relates the permeability enhancement (due to the gas slippage) to the dimensionless Knudsen number of the system. After generation of this plot, it is possible to compare it with Figure 3 which obtained from the experimental measurements for shale rock samples. From the comparison, the proposed boundary conditions can be evaluated for the lattice Boltzmann modelling of gas flow in shale rocks.

For this purpose, gas flow in a long microchannel was simulated and the DR and BSR boundary conditions were used. To generate the general slip plot, the gas flow was simulated at different Knudsen numbers. The characteristic length of the system (channel width) and gas viscosity were altered to change the Knudsen number of the system. It is noted that the channel width and the gas viscosity are corresponding to the characteristic length of the rock and the pore pressure of the flowing gas (in macroscopic scale), respectively. For each simulation, the permeability of the channel was calculated from the obtained average streamwise velocity.

For calculation of the permeability enhancement (K_D), the obtained channel permeability for slip and non-slip flow were used. In other words, the gas flow was simulated with and without slip boundary conditions, i.e. the results with DR and BSR boundary conditions representing slip flow were compared with those with the bounce-back (BB) boundary condition describing the non-slip flow. For the non-slip flow case, the simulation results were double checked by the non-slip N-S solution. For all simulations, the inlet/outlet density ratio ($\frac{\rho_{in}}{\rho_{out}}$) was selected as 1.02.

Figure 8 presents the simulation results of dimensionless permeability of a microchannel at different Knudsen numbers when different boundary conditions were used. As can be seen in this figure, the simulation results of BSR-LBM with $\sigma = 0.8$ are similar to DR-LBM results. However both of them underestimate the permeability of porous media at different Knudsen numbers. As seen in Figure 8 the permeability enhancements obtained by these two boundary conditions (DR-LBM and BSR-LBM with $\sigma = 0.8$) are less than the measured values in porous media. In other words, the slippage intensity in porous media is higher than the predicted gas slippage by these two boundary conditions. Therefore, the TMAC value of 0.8, which was suitable for slip flow in a single microchannel (as shown in Figure 8) is not proper for simulation of gas flow in shale rocks. This could be the main reason for the poor performance of the available permeability predictions model in the literature since almost all of them have been developed assuming gas flow in a single pipe or a single channel. In addition,

these models have never been compared with experimental data performed on porous media.

In order to increase the slippage intensity on the wall surface, the input TMAC is reduced to 0.6 (i.e. shifting the gas collisions towards the fully specular). As illustrated in Figure 8 the experimental data can be better predicted by $\sigma = 0.6$. It means that, to account the gas slippage in shale rocks, the flow can be approximated by using a single pipe/channel model provided that the TMAC of 0.6 is used. In other words, the TMAC of 0.6 can simulate the solid-gas interaction in shale rocks more accurately, if a single pipe/channel is assumed. However, from $Kn > 0.1$, the predicted permeability enhancements by BSR-LBM with $\sigma = 0.6$ start to deviate from the experimental data and overestimate the permeability. It highlights the difference between the gas flow in a single channel and porous media which is more dominant for the Knudsen numbers greater than 0.1. To investigate this, gas flow in a simplified porous media consists of a pore body/ pore throat (P/T) system was simulated and the results were compared with those obtained for gas flow in a single channel.

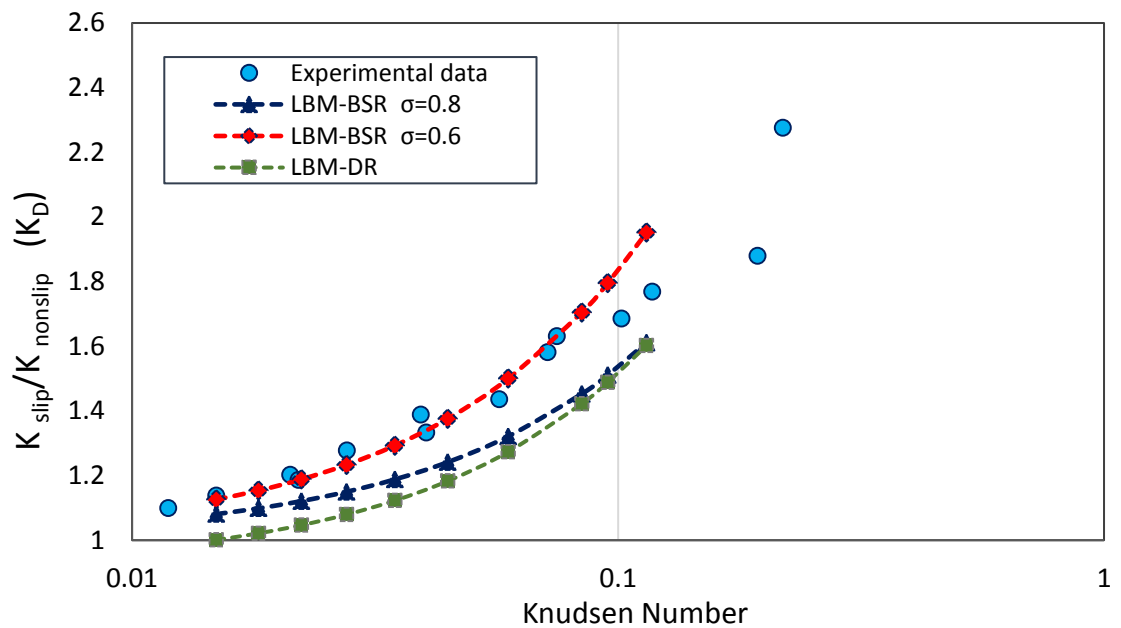


Figure 8: Dimensionless permeability versus Knudsen number; comparison of experimental data and simulation results for gas flow in single channel with different boundary conditions.

Slip Flow in 2D Pore Body/Pore Throat System

In this section, slip flow is simulated in a “pore body/ pore throat” system (P/T system) to study the gas slippage in non-uniform flow paths which is more close to the gas flow in porous media. As mentioned, it is aimed to determine the possible differences between slip flow in a single channel and a simple porous medium network.

The simulation results of slip flow in P/T system were then compared with the obtained results for gas flow in a single channel and experimental data. This kind of comparison can help for better understanding of slip flow in porous media.

When modelling gas flow in porous media, selection of an appropriate characteristic length for the flow conduit attracts many discussions because there are different ranges of pore and throat sizes. The value of the Knudsen number depends on the assigned characteristic length for that porous media. In other words, having variable characteristic length results in variable values of Knudsen number. In this section, this ambiguity is investigated using the simulation results in the P/T system and the experimental data.

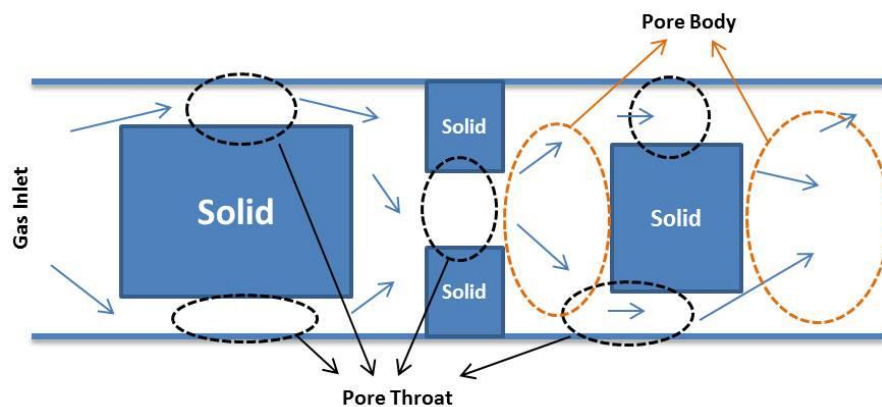


Figure 9: Schematic of the pore body/pore throat system used in this study.

Figure 9 shows the schematic of P/T system used in this study. The slippage on wall surface was modelled by using the BSR boundary conditions. The TMAC was also considered as 0.6 based on the discussion presented in the previous section. As mentioned before, the permeability was obtained based on the Darcy law using the total flow rate at the outlet. The dimensionless permeability factor (K_D) was also calculated from the slip and non-slip flow simulations. In other words, for slip flow, the gas stream in P/T system was simulated with the BSR boundary condition (with $\sigma = 0.6$). For non-slip flow, bounce back (BB) boundary conditions were used to address the gas-wall interaction. It is noted that the boundary conditions were applied for all wall surfaces including the surface of the solid particles. For all simulations, the density ratio was selected as 1.02 and the length of channel was 112 lattice unit (lu). As shown in Figure 9, the dimensions of the solid particles (representative of grains in porous media) were randomly selected to have different pore body and pore throat sizes. Knudsen numbers were also calculated based the obtained characteristic length from 1) pore bodies and 2) pore throats. In other words, for each simulation, the characteristic length of the system

is calculated based on 1) the average value of pore body sizes and 2) the average value of pore throat sizes. As mentioned, it is aim to find out which size is suitable for calculation of system's Knudsen number and can capture the slip behaviour accurately.

The velocity profile obtained from gas flow simulation in the P/T system is shown in Figure 10. In this case, the BSR boundary conditions were used and the obtained permeability was twice of that obtained from the non-slip simulation with BB boundary conditions. As seen in this figure, the gas particles' velocity increase when passing through the pore throats. This enhanced velocity can be even increased due to the gas slippage on the wall surface. Since the gas molecules experience more wall collisions in this area, it can be concluded that the gas slippage on the pore throat walls can probably play more important role in the permeability enhancement. For this case shown in Figure 10, the Knudsen numbers were calculated as 0.0842 and 0.1892 assuming "average pore body sizes" and "average pore throat sizes", respectively. As obtained, the calculated Kn number from the pore throats can be greater than twice of the calculated Kn number from the pore bodies. However this difference depends on the aspect ratio (ratio of the pore body size to the pore throat size) and can be even higher in real porous media. Therefore, it is necessary to know the suitable characteristic length of the flow path as it can be significantly different depends on the average pore size or average throat size. In the following, this point is investigated using the simulation results and the experimental data.

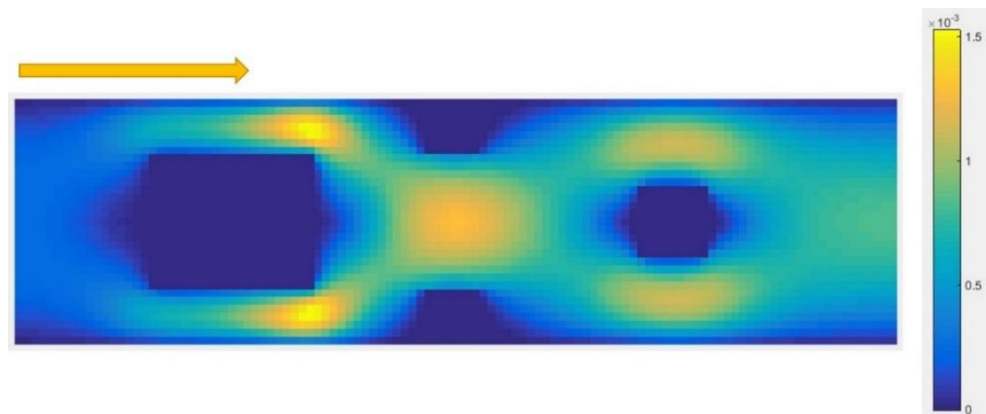


Figure 10: The velocity profile of the gas particles obtained from the LBM simulation of slip flow in the P/T system.

The results of LBM simulations of gas flow in the P/T system for different values of Kn numbers are presented in Figure 11. As shown in this figure, the obtained permeability enhancement factor (K_D) were plotted versus the calculated Kn numbers

from 1) pore bodies and 2) pore throats. In addition, the experimental results are compared with both cases. As can be seen, the experimental data are in good agreement with the predicted permeability enhancements plotted versus Kn numbers obtained from the average pore throats. It means that the matrix permeability can be better predicted when the system is characterized based on the pore throat sizes rather than pore body sizes. It indicates that the porous media length scale, which has the dominant effect on the velocity enhancement, is the average of pore throat sizes not the pore body sizes.

From this exercise, it can be found that the observed permeability enhancement in porous media is mainly because of the gas slippage on throat wall surfaces. In other words, the resistance to pass through the pore throats [which is the main reason of fluid pressure drop (Lei et al. 2007)] is reduced due to the gas slippage. Therefore the gas flow can be alleviated when passing through the pore throats which results in a lower pressure drop and hence a higher permeability.

It is noted that, the simulation results of the P/T system shown in Figure 11 were in good agreement with the experimental data when the aspect ratio of the P/T system was ~ 2.5 . It can be found that the appropriate aspect ratio for simulation of slip flow in the shale samples under study is ~ 2.5 . This ratio is close to the physical values obtained from the gas-adsorption and MICP experiments (Kuila, Prasad 2013).

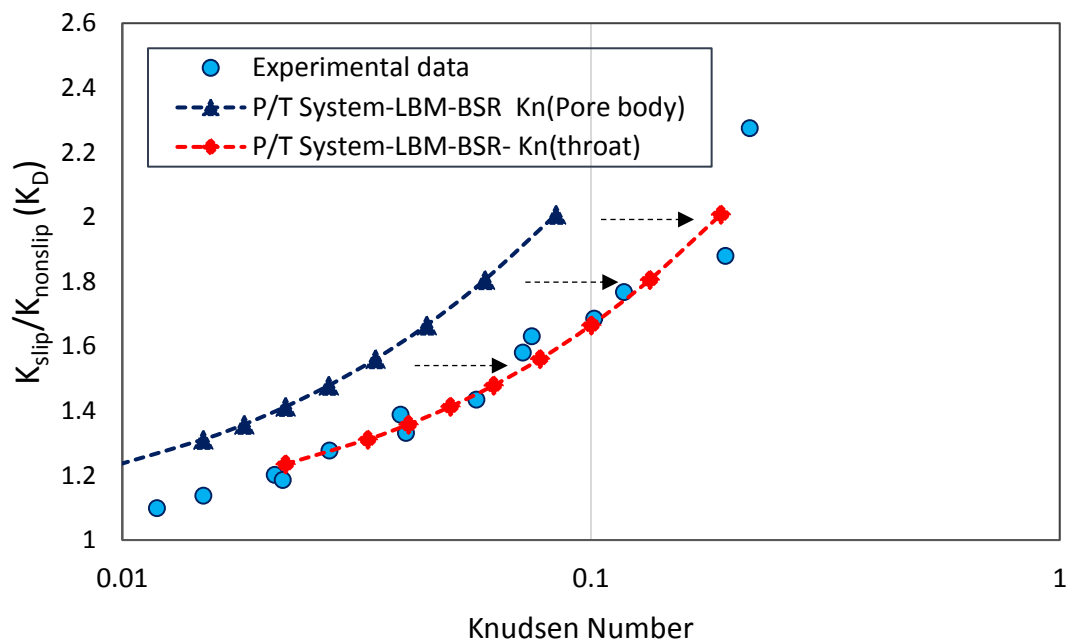


Figure 11: Comparison of experimental data and simulation results of dimensionless permeability as a function of Knudsen number obtained from LBM modelling of the pore body/throat system with different characteristic length.

In addition, the simulation results of gas flow in the P/T system were compared with those obtained in a single channel. It should be noted that for the P/T system, the Knudsen number is calculated based on the average throat sizes. Figure 12 shows the simulated permeability enhancement factor (K_D) versus Knudsen number of the system for a single channel and for the P/T system. As illustrated in this figure, for $Kn > 0.05$, the predicted permeability for a single channel is higher than the predicted values for the P/T system. This could be the main reason for the permeability overestimation of the literature models; e.g. B-K model (Nazari Moghaddam, Jamiolahmady 2016b). In other words, as these models are originally developed based on assumption of flow in a single pipe/channel, they always overestimate the permeability of porous media.

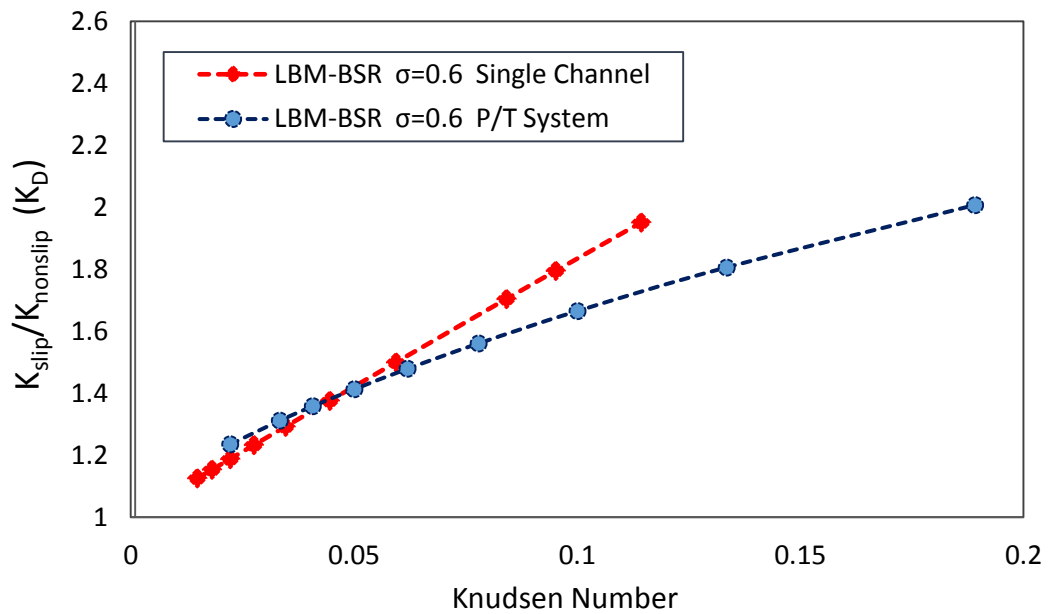


Figure 12: The LBM predicted permeability enhancements versus Knudsen number of the system for a single channel (rotated squares) and the P/T system (circles). For all simulations the BSR (with $TMAC=0.6$) boundary condition was used.

In Figure 13, the experimental data of permeability enhancements are compared with the predicted values obtained from LBM simulation of slip flow in a single channel and in the P/T system. As can be seen in this figure, for higher Knudsen numbers (i.e. $Kn > 0.1$), the flow behaviour in these shale rocks can be better captured when a system of pores/throats are considered. In other words, the permeability enhancement is overestimated for $Kn > 0.1$ when the gas flow is simulated in a single micropipe or microchannel. This overestimation is also given when the analytical models (which are originally developed for a single pipe) are used for shale matrix permeability prediction.

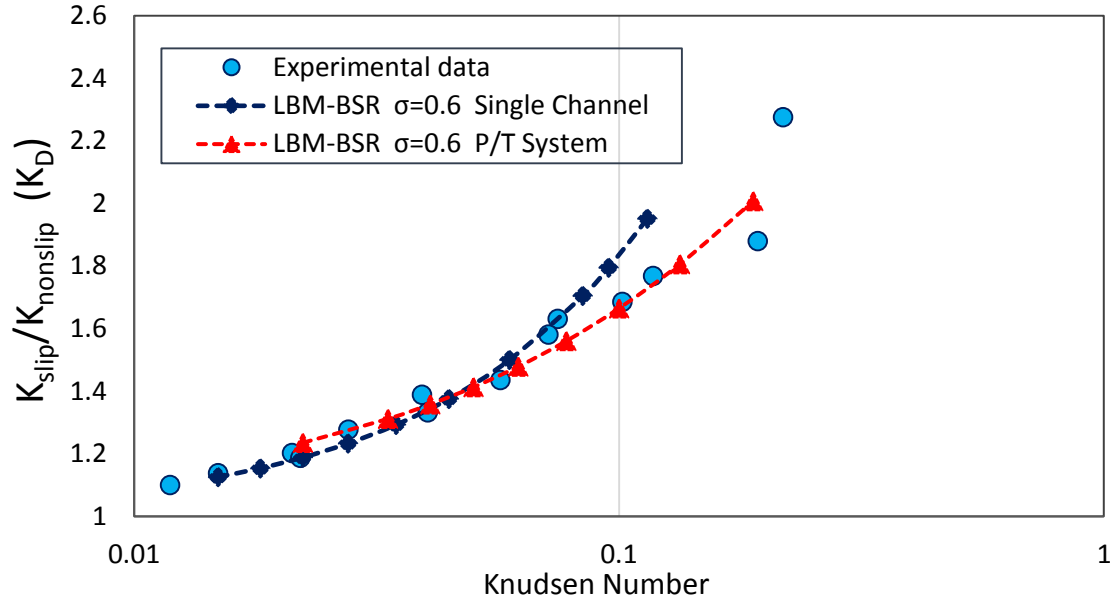
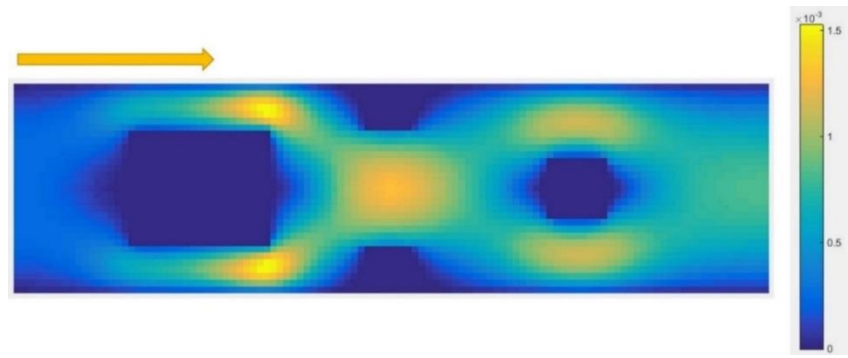


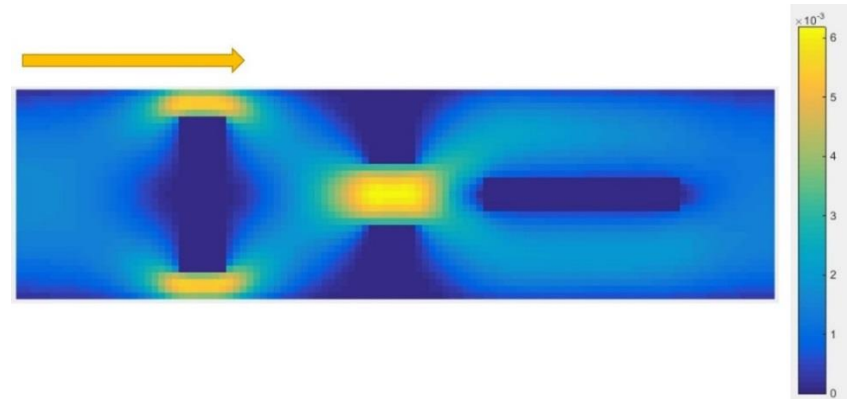
Figure 13: The measured permeability enhancement of shale rocks at various Knudsen numbers compared with the predicted values using LBM simulation of gas flow in a single channel and in the T/P system.

Effects of P/T Structure on the Simulation Results

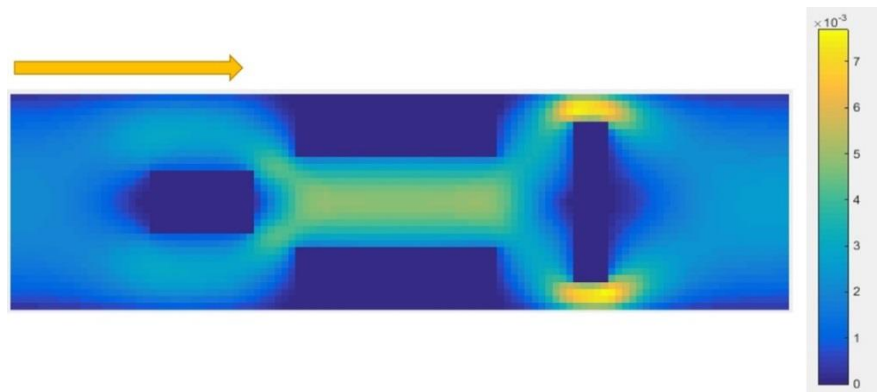
In this section, the gas flow in different configurations of the P/T system were simulated using the BSR boundary conditions. It was aimed to evaluate the effects of the P/T structure on the obtained simulation results. To generate different configurations, the dimensions of the solid particles (see Figure 9) were changed. In all cases, the density ratio (inlet/outlet) and the aspect ratio were 1.02 and 2.5, respectively. The velocity profiles obtained for a typical simulation in these three structures are shown in Figure 14. As shown, different velocity profiles were obtained when the gas flow was simulated in these three P/T configurations. To evaluate the effects of pore structure on the permeability enhancement factor, the gas flow was simulated in these three configurations using bounce-back (for non-slip flow) and BSR boundary conditions (for slip flow). The obtained permeability were used to calculate the dimensionless permeability factor (K_D). The obtained permeability enhancements factors were plotted versus the Knudsen number of the system to generate the general slip plot. It is noted that boundary conditions were applied for the wall surfaces of solid particles.



(a)



(b)



(c)

Figure 14: The velocity profile of the gas flow in three different configurations generated to study the effect of P/T structure on the permeability enhancement factors.

The obtained permeability enhancement factors (K_D) were plotted versus Knudsen number of the system in Figure 15. As shown in this figure, similar permeability enhancement factors were obtained for three cases. It shows that the impact of P/T structure on the permeability enhancement factors are minimal.

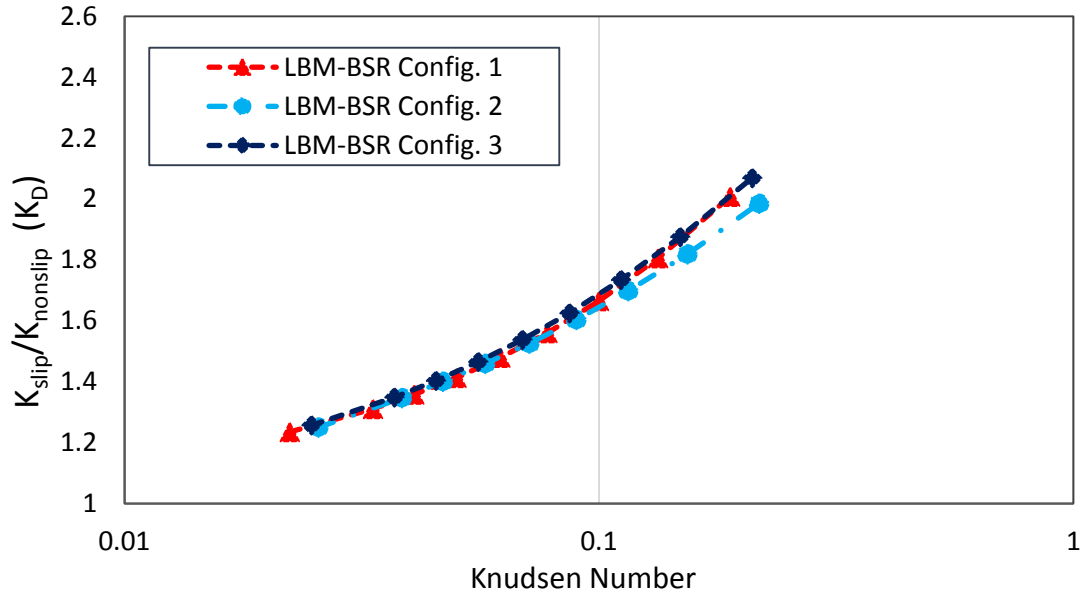


Figure 15: The dimensionless permeability factors versus Knudsen numbers obtained from the LBM-BSR simulations of gas flow in three different P/T configurations shown in Figure 5.10.

Slip Flow in a Randomly Generated 3D Porous Medium

To make the system under study closer to the reality, the gas slippage in a synthetic porous media was studied. The simulations were further extended to performed in a randomly generated porous media using D3Q19 LBM. The flow was simulated in a box-shaped conduit with randomly generated cuboid obstacles as shown in Figure 16. The obstacles were randomly distributed within the conduit. The sizes of the cuboid were also randomly selected. The BSR boundary conditions were applied to capture the fluid-solid interaction on wall surfaces including all obstacle faces and conduit walls. The TMAC was considered as 0.6 based on the discussion presented in the previous section. Similar to 2D simulations, the dimensionless permeability factor (K_D) was also calculated from the slip and non-slip flow simulations. In other words, the ratio of conduit permeability values was obtained when the simulations were conducted with the bounce back and BSR boundary conditions for non-slip and slip flow, respectively.

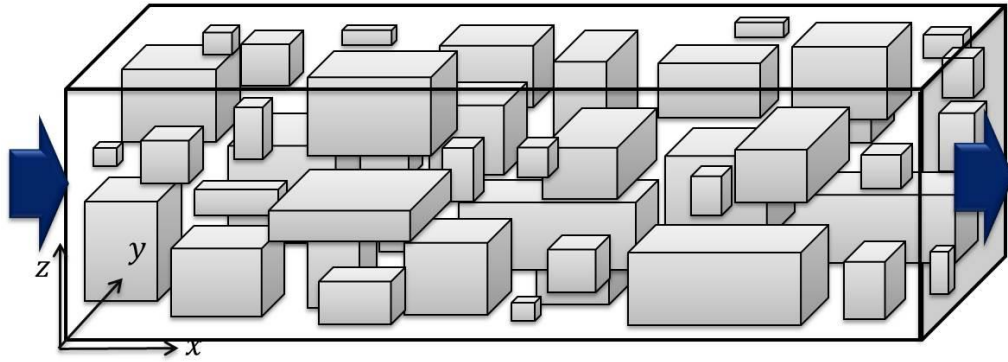


Figure 16: A box-shaped conduit with randomly generated cuboid obstacles used for slip flow simulation by D3Q19 LBM.

The obtained permeability enhancement (K_D) for various Knudsen numbers are presented in Figure 17. In addition, the experimental data and the 2D simulation results of gas flow in P/T systems are also shown. As illustrated, the obtained 3D results also are in good agreement with experimental data. It can be concluded that the LBM simulation technique can capture gas slippage intensity in porous media provided that the appropriate TMAC was selected. It is noted that when using dimensionless permeability (ratio of rock permeability with slippage to rock permeability without slippage, i.e. $K_{slip}/K_{nonslip}$) all other parameters related to medium structure including pore size distribution, pore connectivity and tortuosity, etc. are kept constant. Therefore, the obtained results are not function of these properties. In addition, 2D and 3D simulation results are almost the same because the dimensionless permeability is function of Knudsen number only. It is noted that, as mentioned before, the aspect ratio (which is also a dimensionless number) is also assumed to be the same for all cases.

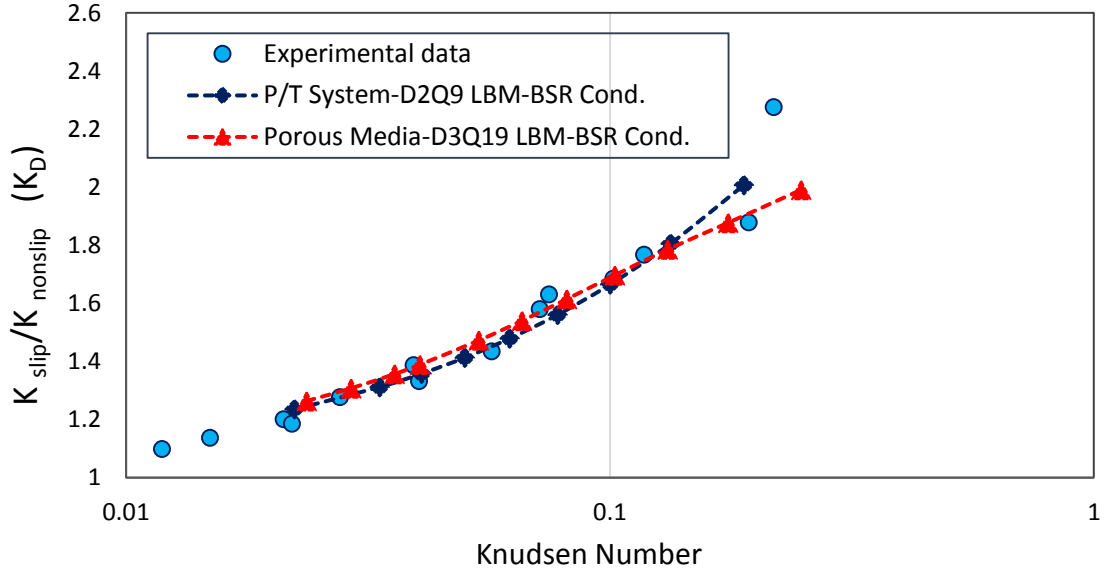


Figure 17: The measured dimensionless permeability (K_D) of shale rocks at various Knudsen numbers compared with the predicted values obtained from LBM simulation of gas flow in a synthetic porous media.

Slip Coefficients of N-S Equations from LBM-BSR Results

In this section, the LBM simulation results of gas flow in the pore body/pore throat system with slip boundary conditions were used to obtain the slip coefficient in the N-S equation. As extensively discussed in the literature (Barisik, Beskok 2011; Zhang et al. 2010; Roy et al. 2003; Lockerby, Reese 2008; Dongari et al. 2007), the N-S equations with slip boundary conditions can approximately predict the flow behaviour in the slip flow regime. As the gas flow in shale and tight reservoirs are mainly within the slip and transition regimes, the N-S equation can be used to predict the permeability enhancement in such systems. Solving the N-S equation with a second-order slip boundary condition gives the following dimensionless permeability expression:

$$K_D = \frac{k_{app}}{k_{non-slip}} = [1 + 4C_1Kn - 8C_2Kn^2] \quad (20)$$

where C_1 and C_2 are the first and second order slip coefficients, respectively. These coefficients can be obtained from the results of gas flow simulations. As shown in Figure 17, the 2D and 3D LBM simulation results are reasonably validated by the experimental data. Afterwards, the simulation results performed for a wider range of Knudsen number can be used for determination of slip coefficients in Equation 20. It is noted that more data for a wider range of Knudsen numbers can be obtained by performing LBM simulations. These results are shown in Figure 18. From the fitted line

of the simulation results in Figure 18, the first and second order slip coefficients are found as 2 and 1.54, respectively. As indicated, these slip coefficients can be used for gas flow prediction when $Kn < 0.3$. Considering the obtained slip coefficients above, the following slip boundary condition is proposed for using the N-S equation to describe the slip flow in these shale rocks:

$$u_s = 2\lambda \left(\frac{\partial u_s}{\partial n} \right)_s + 1.5 \lambda^2 \left(\frac{\partial^2 u_s}{\partial n^2} \right)_s \quad (21)$$

where u_s is the slip velocity, n is the coordinate normal to the wall and λ is the gas mean free path. In addition, the predicted permeability enhancement factors obtained from LBM were compared with those obtained from the Klinkenberg model. As illustrated in this figure, the Klinkenberg model, which is a first-order slip model, overestimates the permeability enhancement. That is, as shown, for $Kn > 0.05$, the first order slip models (e.g. Klinkenberg model) cannot be applied on the experimental data. In other words, for those experiments performed at the pressure conditions with $Kn > 0.05$, the Klinkenberg model cannot be applied to extract the non-slip permeability. Therefore, for using Klinkenberg model, it is required to perform the experiments above a certain pressure (depending on the characteristic length of the system) which gives the system's Knudsen number less than 0.05.

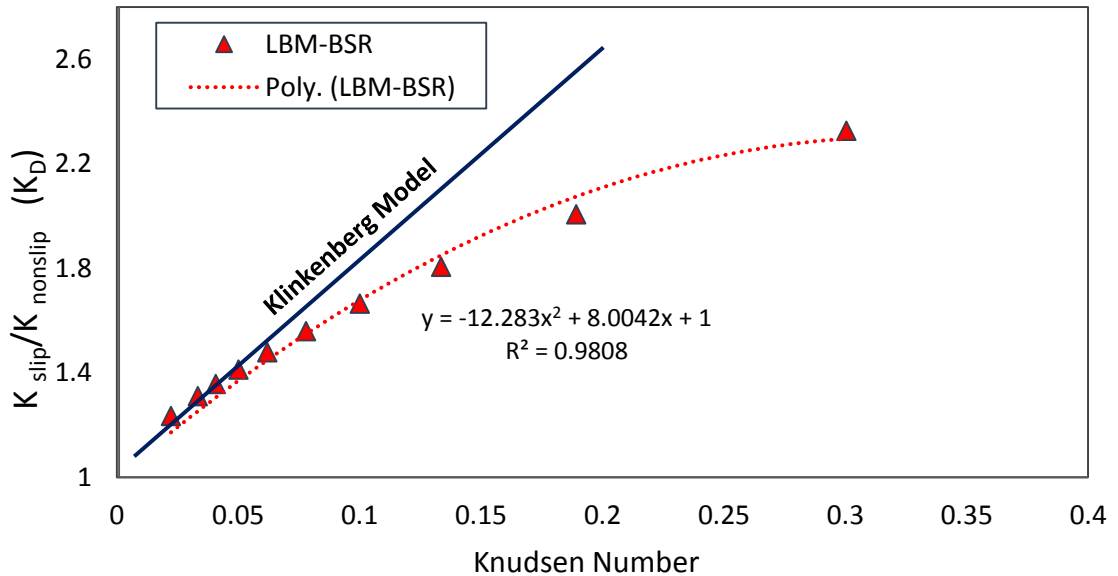


Figure 18: Simulation results of dimensionless permeability as a function of Knudsen number obtained from LBM modelling of a pore body/throat system. The second-order slip coefficients can be obtained from the results.

Summary and Conclusion

In this paper, two-relaxation-time based Lattice Boltzmann Method (TRT-LBM) was used to simulate the gas flow. Different boundary conditions were applied to capture the gas slippage at the wall surface. First, the simulation results of LBM for non-slip flow were validated based on the solutions of N-S equations. In addition, for slip flow, the reliability of the LBM results with DR and BSR boundary conditions were also confirmed based on the solution of other methods found in the literature (IP and DSMC). After validation, slip gas flow was simulated and compared with the measured permeability data of three shale rocks in slip and transition regimes. The effects of different slip boundary conditions and various accommodation coefficients were studied. In addition, gas flow in a system of pore body/pore throat (P/T) was modelled and the simulation results were compared with those obtained for gas flow in a single channel. Furthermore, the simulation results of gas flow in the P/T system and a simplified 3D porous medium were compared with the experimental data. Finally, the LBM simulation results were used to propose appropriate slip coefficients for N-S equation for a wider range of Knudsen numbers. The following observations/conclusions can be made/drawn from this study:

- It was shown that gas slippage for three shale rocks under study, could not be captured by LBM simulations when gas flow is simulated in a single channel and the diffusive reflection (DR) boundary conditions are used. That is, the results of LBM-DR underestimated the permeability enhancement.
- The slippage intensity obtained from the LBM simulation of gas flow in a single channel using BSR boundary condition with the literature value of $TMAC=0.8$ also less than the measured permeability enhancement in three shale samples. It was found that the $TMAC$ of 0.6 could better estimate the permeability enhancement.
- It was shown that the characteristic length of porous media can be better described by the average of pore throat sizes rather than average of pore body sizes. In addition, it was concluded that the gas slippage on the wall surface of the pore throats has significant impacts on the flow enhancement. This is mainly because of the pressure drop reduction across the pore throat which is due to the relative ease of flow with slippage.

- Furthermore, the simulation results of slip flow in a single channel were compared with those obtained for flow in the P/T system. From the comparison, it was found that, for $Kn > 0.05$, the LBM simulation of slip flow in a single channel gives higher permeabilities compared to those values obtained from the LBM simulation in the P/T system.
- Moreover, the experimental data could be better simulated when the P/T system was considered. It means that the permeability enhancement is overestimated for $Kn > 0.1$ when the gas flow is simulated in a single micropipe or microchannel. It was concluded that the main reason for the matrix permeability overestimation of the literature models can be due to the assumption of flow in a single pipe/channel.
- In addition, gas flow in a simplified 3D porous medium was simulated using D3Q19 LBM. The obtained results confirmed those obtained from P/T system. Also, reasonable agreement was obtained when the 3D simulation results were compared with the scaled experimental data.
- From the fitted line to the simulation results (up to $Kn = 0.3$), the first and second order slip coefficients of the N-S boundary condition were proposed as 2 and 1.54, respectively. Also, it was found that first order slip model including Klinkenberg model can give errors when it applies on the experimental data measured at the pressure conditions which gives $Kn > 0.05$.

List of Symbols

Nomenclature

n	coordination normal to the wall
C_1	first-order slip coefficient
C_2	second-order slip coefficient
u	velocity in x-direction
f	particle distribution function
f^{eq}	Boltzmann-Maxwell distribution function
t	time
ξ	particle velocity
m	molecular mass

c	lattice speed
c_s	speed of sound
t	time
x	direction
T	temperature
K	absolute permeability

Greek Letters

ρ	density
λ	mean free path of flowing gas
μ	viscosity
α	direction of velocity $\alpha = 1, \dots, 8, 9$,
Ω	collision term
σ	tangential momentum accommodation coefficient
ζ	particle velocity
ν	kinematic viscosity

Subscript

w	wall
app	apparent
non-slip	without slip
s	slip
D	dimensionless
w	wall
out	outlet

Abbreviations

Kn	Knudsen number
DSMC	direct simulation Monte Carlo
MD	molecular dynamic
DGM	dusty gas model
B-K	Beskok and Karniadakis
KL	Knudsen Layer
TMAC	tangential momentum accommodation coefficient
IP	information preservation

MFP	mean free path
N-S	Navier-Stokes
SRT	single relaxation time
TRT	two relaxation time
MRT	multi relaxation time
BB	bounce-back boundary condition
SR	specular reflection boundary condition
DR	diffusive reflection boundary condition
BSR	bounce back-specular reflection
lu	lattice unit

Acknowledgements

This study was conducted as a part of the Unconventional Gas and Gas-condensate Recovery Project at Heriot-Watt University. This research project is sponsored by: Daikin, Dong Energy, Ecopetrol/Equion, ExxonMobil, GDF, INPEX, JX-Nippon, Petrobras, RWE, Saudi-Aramco and TOTAL, whose contribution is gratefully acknowledged.

References

- Asinari, P.: Multi-Scale Analysis of Heat and Mass Transfer in Mini/Micro-Structures. Ph. D. Dissertation (2005)
- Bao, Y.B., Meskas, J.: Lattice Boltzmann method for fluid simulations. Department of Mathematics, Courant Institute of Mathematical Sciences, New York University (2011)
- Barisik, M., Beskok, A.: Molecular dynamics simulations of shear-driven gas flows in nano-channels. *Microfluidics and nanofluidics* **11**(5), 611-622 (2011)
- Beskok, A., Karniadakis, G.E.: Report: a model for flows in channels, pipes, and ducts at micro and nano scales. *Microscale Thermophysical Engineering* **3**(1), 43-77 (1999)
- Bhatia, S.K., Bonilla, M.R., Nicholson, D.: Molecular transport in nanopores: a theoretical perspective. *Physical Chemistry Chemical Physics* **13**(34), 15350-15383 (2011)
- Bhatia, S.K., Nicholson, D.: Molecular transport in nanopores. *The Journal of Chemical Physics* **119**(3), 1719-1730 (2003). doi:doi:<http://dx.doi.org/10.1063/1.1580797>
- Cercignani, C.: *Rarefied gas dynamics: from basic concepts to actual calculations*, vol. 21. Cambridge University Press, (2000)
- Civan, F.: Effective correlation of apparent gas permeability in tight porous media. *Transport in porous media* **82**(2), 375-384 (2010)
- Darabi, H., Etehad, A., Javadpour, F., Sepehrnoori, K.: Gas flow in ultra-tight shale strata. *Journal of Fluid Mechanics* **710**, 641-658 (2012)
- Deng, J., Zhu, W., Ma, Q.: A new seepage model for shale gas reservoir and productivity analysis of fractured well. *Fuel* **124**, 232-240 (2014)
- Dongari, N., Agrawal, A., Agrawal, A.: Analytical solution of gaseous slip flow in long microchannels. *International Journal of Heat and Mass Transfer* **50**(17), 3411-3421 (2007)

- Ewart, T., Perrier, P., Graur, I., Méolans, J.G.: Tangential momentum accommodation in microtube. *Microfluidics and Nanofluidics* **3**(6), 689-695 (2007)
- Fathi, E., Akkutlu, I.Y.: Lattice Boltzmann Method for Simulation of Shale Gas Transport in Kerogen. *Society of Petroleum Engineers Journal* **18**(01) (2013). doi:10.2118/146821-PA
- Fathi, E., Tinni, A., Akkutlu, I.Y.: Correction to Klinkenberg slip theory for gas flow in nano-capillaries. *International Journal of Coal Geology* **103**, 51-59 (2012)
- Florence, F.A., Rushing, J., Newsham, K.E., Blasingame, T.A.: Improved Permeability Prediction Relations for Low Permeability Sands. Paper presented at the Rocky Mountain Oil & Gas Technology Symposium, Denver, Colorado, U.S.A., 2007/1/1/
- Freeman, C., Moridis, G., Blasingame, T.: A numerical study of microscale flow behavior in tight gas and shale gas reservoir systems. *Transport in porous media* **90**(1), 253-268 (2011)
- Ghanizadeh, A., Gasparik, M., Amann-Hildenbrand, A., Gensterblum, Y., Krooss, B.M.: Experimental study of fluid transport processes in the matrix system of the European organic-rich shales: I. Scandinavian Alum Shale. *Marine and Petroleum Geology* **51**, 79-99 (2014)
- Ginzburg, I.: Equilibrium-type and link-type lattice Boltzmann models for generic advection and anisotropic-dispersion equation. *Advances in Water resources* **28**(11), 1171-1195 (2005)
- Ginzburg, I., Verhaeghe, F., d'Humieres, D.: Study of simple hydrodynamic solutions with the two-relaxation-times lattice Boltzmann scheme. *Communications in computational physics* **3**(3), 519-581 (2008)
- Graur, I., Perrier, P., Ghozlani, W., Méolans, J.: Measurements of tangential momentum accommodation coefficient for various gases in plane microchannel. *Physics of Fluids* **21**(10), 102004 (2009)
- Guo, C., Xu, J., Wu, K., Wei, M., Liu, S.: Study on gas flow through nano pores of shale gas reservoirs. *Fuel* **143**, 107-117 (2015)
- Guo, Z., Zhao, T., Shi, Y.: Physical symmetry, spatial accuracy, and relaxation time of the lattice Boltzmann equation for microgas flows. *Journal of Applied physics* **99**(7), 074903 (2006)
- Guo, Z., Zheng, C., Shi, B.: Lattice Boltzmann equation with multiple effective relaxation times for gaseous microscale flow. *Physical Review E* **77**(3), 036707 (2008)
- Heller, R., Vermilyen, J., Zoback, M.: Experimental investigation of matrix permeability of gas shales. *AAPG bulletin* **98**(5), 975-995 (2014)
- Homayoon, A., Isfahani, A.M., Shirani, E., Ashrafizadeh, M.: A novel modified lattice Boltzmann method for simulation of gas flows in wide range of Knudsen number. *International Communications in Heat and Mass Transfer* **38**(6), 827-832 (2011)
- Javadpour, F.: Nanopores and Apparent Permeability of Gas Flow in Mudrocks (Shales and Siltstone). *J Can Petrol Technol* **48**(08) (2009). doi:10.2118/09-08-16-DA
- Kang, S.M., Fathi, E., Ambrose, R.J., Akkutlu, I.Y., Sigal, R.F.: Carbon Dioxide Storage Capacity of Organic-Rich Shales. (2011). doi:10.2118/134583-PA
- Kuila, U., Prasad, M.: Specific surface area and pore-size distribution in clays and shales. *Geophysical Prospecting* **61**(2), 341-362 (2013)
- Lei, Q., Xiong, W., Yuang, J., Cui, Y., Wu, Y.-S.: Analysis of stress sensitivity and its influence on oil production from tight reservoirs. In: Eastern Regional Meeting 2007. Society of Petroleum Engineers

- Li, Q., He, Y., Tang, G., Tao, W.: Lattice Boltzmann modeling of microchannel flows in the transition flow regime. *Microfluidics and nanofluidics* **10**(3), 607-618 (2011)
- Lim, C., Shu, C., Niu, X., Chew, Y.: Application of lattice Boltzmann method to simulate microchannel flows. *Physics of Fluids (1994-present)* **14**(7), 2299-2308 (2002)
- Lockerby, D.A., Reese, J.M.: On the modelling of isothermal gas flows at the microscale. *Journal of Fluid Mechanics* **604**, 235-261 (2008)
- Luo, L.-S.: Comment on "Discrete Boltzmann equation for microfluidics". *Physical review letters* **92**(13), 139401 (2004)
- Luo, L.-S.: Comment on "Heat transfer and fluid flow in microchannels and nanochannels at high Knudsen number using thermal lattice-Boltzmann method". *Physical Review E* **84**(4), 048301 (2011)
- Maurer, J., Tabeling, P., Joseph, P., Willaime, H.: Second-order slip laws in microchannels for helium and nitrogen. *Physics of Fluids* **15**(9), 2613-2621 (2003)
- Mohamad, A.A.: Lattice Boltzmann method: fundamentals and engineering applications with computer codes. Springer Science & Business Media, (2011)
- Nazari Moghaddam, R., Jamiolahmady, M.: Fluid transport in shale gas reservoirs: Simultaneous effects of stress and slippage on matrix permeability. *International Journal of Coal Geology* **163**, 87-99 (2016a)
- Nazari Moghaddam, R., Jamiolahmady, M.: Slip flow in porous media. *Fuel* **173**, 298-310 (2016b)
- Nie, X., Doolen, G.D., Chen, S.: Lattice-Boltzmann simulations of fluid flows in MEMS. *Journal of Statistical Physics* **107**(1-2), 279-289 (2002)
- Ning, Y., Jiang, Y., Liu, H., Qin, G.: Numerical modeling of slippage and adsorption effects on gas transport in shale formations using the lattice Boltzmann method. *Journal of Natural Gas Science and Engineering* **26**, 345-355 (2015)
- Niu, C., Hao, Y.-z., Li, D., Lu, D.: Second-Order Gas-Permeability Correlation of Shale During Slip Flow. *SPE Journal* **19**(05), 786-792 (2014)
- Niu, X., Shu, C., Chew, Y.: A lattice Boltzmann BGK model for simulation of micro flows. *EPL (Europhysics Letters)* **67**(4), 600 (2004)
- Ren, J., Guo, P., Guo, Z., Wang, Z.: A Lattice Boltzmann Model for Simulating Gas Flow in Kerogen Pores. *Transport in Porous Media* **106**(2), 285-301 (2015)
- Roy, S., Raju, R., Chuang, H.F., Cruden, B.A., Meyyappan, M.: Modeling gas flow through microchannels and nanopores. *Journal of applied physics* **93**(8), 4870-4879 (2003)
- Sakhaee-Pour, A., Bryant, S.: Gas Permeability of Shale. *SPE Reservoir Evaluation & Engineering* **15**(04), 401-409 (2012). doi:10.2118/146944-PA
- Satoh, A.: Introduction to practice of molecular simulation: molecular dynamics, Monte Carlo, Brownian dynamics, Lattice Boltzmann and dissipative particle dynamics. Elsevier, (2010)
- Sbragaglia, M., Succi, S.: Analytical calculation of slip flow in lattice Boltzmann models with kinetic boundary conditions. *Physics of Fluids (1994-present)* **17**(9), 093602 (2005)
- Shen, C., Tian, D.-B., Xie, C., Fan, J.: Examination of the LBM in simulation of microchannel flow in transitional regime. *Microscale Thermophysical Engineering* **8**(4), 423-432 (2004)
- Shokouhmand, H., Isfahani, A.M.: An improved thermal lattice Boltzmann model for rarefied gas flows in wide range of Knudsen number. *International Communications in Heat and Mass Transfer* **38**(10), 1463-1469 (2011)

- Sinha, S., Braun, E., Determan, M., Passey, Q., Leonardi, S., Boros, J., Wood III, A., Zirkle, T., Kudva, R.: Steady-state permeability measurements on intact shale samples at reservoir conditions-effect of stress, temperature, pressure, and type of gas. In: SPE Middle East Oil and Gas Show and Conference 2013. Society of Petroleum Engineers
- Sofonea, V., Sekerka, R.F.: Boundary conditions for the upwind finite difference Lattice Boltzmann model: Evidence of slip velocity in micro-channel flow. *Journal of Computational Physics* **207**(2), 639-659 (2005)
- Succi, S.: Mesoscopic modeling of slip motion at fluid-solid interfaces with heterogeneous catalysis. *Physical review letters* **89**(6), 064502 (2002)
- Tang, G., Tao, W., He, Y.: Lattice Boltzmann method for gaseous microflows using kinetic theory boundary conditions. *Physics of Fluids (1994-present)* **17**(5), 058101 (2005)
- Tang, G., Zhang, Y., Gu, X., Emerson, D.: Lattice Boltzmann modelling Knudsen layer effect in non-equilibrium flows. *EPL (Europhysics Letters)* **83**(4), 40008 (2008)
- Verhaeghe, F., Luo, L.-S., Blanpain, B.: Lattice Boltzmann modeling of microchannel flow in slip flow regime. *Journal of Computational Physics* **228**(1), 147-157 (2009)
- Yves, G., Amin, G., Robert, C.J., Amann-Hildenbrand, A., Krooss, B.M., Clarkson, C.R., Harrington, J.F., Zoback, M.D.: Gas storage capacity and transport in shale gas reservoirs—A review. Part A: Transport processes. *Journal of Unconventional Oil and Gas Resources* (2015)
- Zhang, H., Zhang, Z., Zheng, Y., Ye, H.: Corrected second-order slip boundary condition for fluid flows in nanochannels. *Physical Review E* **81**(6), 066303 (2010)
- Zhang, X.-L., Xiao, L.-Z., Guo, L., Xie, Q.-M.: Investigation of shale gas microflow with the Lattice Boltzmann method. *Petroleum Science* **12**(1), 96-103 (2015)
- Zhang, Y., Qin, R., Emerson, D.R.: Lattice Boltzmann simulation of rarefied gas flows in microchannels. *Physical Review E* **71**(4), 047702 (2005)
- Zhu, L., Tretheway, D., Petzold, L., Meinhart, C.: Simulation of fluid slip at 3D hydrophobic microchannel walls by the lattice Boltzmann method. *Journal of Computational Physics* **202**(1), 181-195 (2005)
- Ziarani, A.S., Aguilera, R.: Knudsen's permeability correction for tight porous media. *Transport in porous media* **91**(1), 239-260 (2012)
- Zou, Q., He, X.: On pressure and velocity boundary conditions for the lattice Boltzmann BGK model. *Physics of Fluids (1994-present)* **9**(6), 1591-1598 (1997)